JPC-A113-10652-Murakami-xylene-DF-deconpos

DATASET · JULY 2013

4 AUTHORS, INCLUDING:

Yoshio Nosaka
Nagaoka University of Technology
228 PUBLICATIONS **5,723** CITATIONS
SEE PROFILE

Yoshinori Murakami
Nagaoka National College of Technology
38 PUBLICATIONS **593** CITATIONS
SEE PROFILE

Density Functional Study of the High-Temperature Oxidation of *o*-, *m*- and *p*-Xylyl Radicals

Yoshinori Murakami,*,† Tatsuo Oguchi,‡ Kohtaro Hashimoto,§ and Yoshio Nosaka‖

Department of Materials Engineering, Nagaoka National College of Technology, Nishikatagai, Nagaoka, 940-8532 Japan, Department of Ecological Engineering, Toyohashi University of Technology, Toyohashi, 441-8580 Japan, Honda R&D Co. Ltd. Fundamental Technology Research Center, 1-4-1 Chuo, Wako-shi, Saitama, 351-0193 Japan, and Department of Chemistry, Nagaoka University of Technology, Kamitomioka, Nagaoka, 940-2188 Japan

Received: March 11, 2009; Revised Manuscript Received: August 18, 2009

Theoretical calculations at the CBS-QB3 level of theory have been performed to investigate the potential energy surface for the reaction of *o*-, *m*- and *p*-xylyl with molecular oxygen. The differences of the relative potential energies for the products and the transition states of *o*-, *m*- and *p*-xylyl with molecular oxygen were found to be within 8.5 kJ/mol at the CBS-QB3 level of theory. Although the reaction of *m*- and *p*-xylyl radicals with molecular oxygen have the same reaction pathways and also the same reaction thermochemistry as that of benzyl radicals, the *o*-xylylperoxy radicals formed by the reaction of *o*-xylyl + O_2 had an additional intramolecular isomerization pathway to form the *o*-xylyl hydroperoxy radicals. The rate constants and the product branching ratios for the *o*-xylyl + O_2 and its subsequent reactions were evaluated by the RRKM and master equation analysis. Possible roles for these reaction pathways on the combustion of *o*-xylenes are discussed.

1. Introduction

The presence of significant quantities of aromatic hydrocarbons in practical engine fuels makes it important to study the chemistry of aromatic fuels under engine conditions. Since small aromatic compounds such as toluene and xylenes are important automotive fuel components because of the high-energy density and antiknock rating, detailed modeling of combustion for such aromatic hydrocarbons has been investigated. For example, Emdee et al.[1] proposed a kinetic model for the high-temperature oxidation of toluene and reproduced the decay rates of toluene and many intermediate species in a flow reactor around 1200 K. Later, Lindstadt and Maurice[2] developed a more detailed chemical kinetic mechanism of toluene combustion with 743 elementary reactions and 141 species and successfully reproduced the major and intermediate species profiles in diffusion flames, in premixed flames, in plug flow reactors, and in shock tubes over a wide temperature range. They further suggested that benzylperoxy ($C_6H_5CH_2OO$) radicals formed by the addition of molecular oxygen to the benzyl ($C_6H_5CH_2$) radicals play the key roles in toluene combustion at a relatively lower temperature range.

Although several researchers have investigated the rate constants for benzyl + O_2 reaction at high temperatures,[3−5] few works have been carried out for the determination of the product branching ratios for the thermal decomposition of the benzylperoxy radicals formed by the benzyl + O_2 reaction. Clothier et al.[6] first calculated the reaction pathway forming OH radicals and benzaldehyde by thermal decomposition of benzylperoxy radicals using ROMP2//3-21G approximation and suggested that the benzylperoxide radical can act as the effective diesel-fuel ignition improver. Later, Murakami et al.[7] calculated the product branching ratios for all of the plausible reaction channels of the benzyl + O_2 reaction using the CBS-QB3 method combined with RRKM/master-equation analysis. According to these calculations, the product branching ratios of OH radicals formed by decomposition of benzylperoxy radicals were found to be around 0.7 between 300 and 1500 K, which was consistent with the conclusion by Clothier et al. that benzylperoxy radicals act as the ignition improver because of the formation of the chain-initiating OH radicals.

On the other hand, Canneaux et al.[8] calculated the structures of the benzylperoxy radicals and also of the transition states from benzylperoxy ($C_6H_5CH_2OO$) to benzyl hydroperoxide (C_6H_5CHOOH) radical, which again decompose to form benzaldehyde and OH radicals. Although the geometries calculated with the B3LYP, MPW1K, and MP2 methods combined with six different basis sets were consistent with the previous studies of Garcia et al.[9] and Murakami et al.,[7] the barrier height using the elaborated CASPT2 method showed a lower activation barrier (137.1 kJ mol^{-1}) than that of the CBS-QB3 method (161.9 kJ mol^{-1}) by Murakami et al.[7] They also calculated the high-pressure rate constant using the values in the CASPT2 method and found that the rate constant was in good agreement with that obtained by product analysis in toluene/H_2/O_2/N_2 mixtures,[10] although this calculated rate constant was about 200 times larger than that calculated by Murakami et al.[7] Thus, the relative roles of the reaction channel forming OH and benzaldehyde from the benzyl + O_2 reaction were still in debate, and the reaction mechanism and the reaction kinetics for the benzyl + O_2 reaction are now better understood.

Xylenes are also used as constituents in gasolines as well as diesel fuel, but the oxidation mechanism for xylenes is less understood than that of toluene. Gail and Dagout proposed a chemical kinetic modeling of *p*-xylene for the first time that is based on the product analysis in a jet-stirred reactor for temperatures 900−1300 K.[11] At the same time, Battin-Leclerc

* To whom correspondence should be addressed. E-mail: murakami@nagaoka-ct.ac.jp.
† Nagaoka National College of Technology.
‡ Toyohashi University of Technology.
§ Honda R&D Co. Ltd.
‖ Nagaoka University of Technology.

10.1021/jp902204a CCC: $40.75
Published on Web 09/11/2009

et al.[12] measured the autoignition of the three isomers of xylene (*o*-, *m*-, and *p*-xylenes) in a shock tube (1330−1800 K) and found that there were no distinct differences in the ignition delays among these three isomers. They proposed the chemical kinetic modeling of xylene combustion, but their models were guessed from analogies of the combustion of aromatic compounds, and thus, no distinct different chemical kinetic modeling among the three xylene isomers has been proposed.

On the other hand, the different oxidation mechanisms among *o*-, *m*-, and *p*-xylenes has already been suggested by several researchers. Emdee et al.[13] proposed the different oxidation mechanisms between *m*- and *p*-xylenes on the basis of the GC analysis of a atmospheric flow reactor at temperatures 1093−1199 K. They suggested that *m*-xylene is oxidized by sequential oxidation and removal of the methyl side chains, whereas *p*-xylene reacts through simultaneous as well as sequential oxidation of the side chain. Wright[14] found that *o*-xylene oxidized more easily than *m*- and *p*-xylene by measuring the change in pressure as a function of time in a reaction vessel at temperatures of 683−823 K. Barnard and Sankey[15,16] also studied slow oxidation reactions of the *o*-, *m*-, and *p*-xylenes in a static reactor at temperatures between 733 and 785 K. They again found experimentally that *o*-xylene has a higher reactivity than *m*- and *p*-xylenes, and they explained the reasons for the high reactivities of *o*-xylene as the existence of a reaction scheme involving intramolecular hydrogen transfer from the *o*-xylylperoxy radicals. Roubaud et al.[17] studied the autoignition features of 11 alkylbenzenes in a rapid compression machine at temperatures of 600−900 K and pressures up to 25 bar. They found that the autoignition features of alkylbenzenes were classified in two groups. *o*-Xylene, ethylbenzene, 1,2,3-trimethylbenzene, 1,2,4-trimethylbenzene, *n*-propylbenzene, 2-ethyltoluene, and *n*-butylbenzene iginite at a much lower temperature and pressure, and *m*-xylene, *p*-xylene, and 1,3,5-trimethylbenzene ignite only above 900 K and 16 bar. Thus, the higher reactivity of *o*-xylene than *m*- and *p*-xylene was also observed in a rapid compression machine.

Recently, theoretical work on the kinetics for the isomerization reaction of *o*-, *m*- and *p*-xylylperoxy radicals was performed by Canneaux et al.[18] They calculated the barrier heights for the isomerization reaction forming methyl(hydroperoxy)benzyl radicals from the *o*-, *m*-, and *p*-xylylperoxy radicals and also that for the isomerization reaction forming 2-(hydroperoxy)-methylbenzyl radical from *o*-xylylperoxy radical using the elaborated CASPT2 method. They also estimated the rate constant for each reaction with various kinds of theory and concluded that the intramolecular hydrogen transfer reaction to form 2-(hydroperoxy)methylbenzyl radical from the *o*-xylylperoxy radicals was dominant, even below 2000 K. However, in their calculations, only the above two isomerization reaction channels were calculated, and the search for the other isomerization pathways as well as the further decomposition reaction pathways of xylylperoxy radicals after the isomerization reactions of xylylperoxy radicals have not been done.

In the present study, quantum chemical calculations for *o*-, *m*-, and *p*-xylyl radicals with molecular oxygen were performed, and the potential barrier heights for all of the plausible isomerization reaction channels were calculated. Since the CBS-Q calculation was used by several authors for calculation of the isomerization reactions for the hydroperoxy radicals,[19−21] we have also adopted the same level of CBS-QB3 theory to obtain the potential energy diagram. Furthermore, the RRKM and master equation analysis based on these quantum chemical calculations were also carried out to estimate the rate constants and the product branching rations for these reactions. Finally, plausible explanations for the different ignition behaviors between *o*-xylene and *m*- and *p*- xylenes are also presented.

2. Calculation Methods

2.1. Quantum Chemistry Calculations. All quantum chemical computations have been performed with the set of Gaussian-03 suite of programs.[22] The geometries of the reactants, products, various intermediates, and transition states for the reactions of the *o*-, *m*- and *p*-xylyl + O_2 were carried out using density functional theory at the B3LYP/6-311G(2d, p, p) level of theory, followed by analytical frequency calculations at the same level to verify that the stationary points were properly located (one imaginary frequency for a transition state and all positive frequencies for a minimum) and also to determine the zero point energies for the stationary points. The intrinsic reaction coordinate procedure was used to follow the reaction path from the transition state to reactants and products. Potential energies at the stationary points were further refined using the procedures of the complete basis method CBS-QB3 developed by Petersson and co-workers.[23,24] CBS-QB3 is a multilevel model chemistry that combines the results of several electronic structure calculations and empirical terms to predict molecular energies with relatively low computational costs. The required electronic structure calculations are outlined as follows: (i) B3LYP/6-311G(2d,d,p) geometry optimization and frequencies, (ii) MP2/6-311G(3df,2df,2p) energy and CBS extrapolation, (iii) MP4(SDQ)/6-31G(d(f),p) energy; (iv) CCSD(T)/6-31+G(d′) energy. According to the previous investigations,[24] the CBS-QB3 gives gas-phase energies with an average error of approximately 4 kJ mol^{-1}. To confirm the accuracy of the level of the CBS-QB3 theory in the present calculations, the heat of reaction from the benzyl + O_2 reaction to benzylperoxyl radicals has been estimated at the level of the CBS-QB3 theory. The calculated heat of reaction at the level of the CBS-QB3 theory was −92.9 kcal/mol, which was found to be in good agreement with the experimentally obtained heat of reaction, −91.2 kcal/mol.[25]

2.2. Statistical Rate Theory Calculations. Rice−Ramsperger−Kassel−Marcus/master equation (RRKM/ME) calculations were carried out using the UNIMOL program of Gilbert and Smith[26] to obtain thermal rate constants for the multichannel dissociation reactions of xylylperoxy radicals. The microcanonical rate constant, $k(E)$, was calculated from the standard form

$$k(E) = W(E - E_0)/h\,\rho(E) \quad (4)$$

where $W(E)$ denotes the sum of the transition state, E_0 is the corresponding threshold energy, h is Planck's constant, and $\rho(E)$ is the density of states for xylylperoxy radicals. In the present RRKM/ME calculations, the conservation of angular momentum was included only in the case of the high-pressure limit. The Lennard-Jones parameters for all of the *o*-, *m*-, *p*-xylylperoxy radicals were assumed to be the same as those for benzyl alcohol ($C_6H_5CH_2OH$), whose Lennard-Jones parameters were $\sigma = 4.6$ Å and $\varepsilon = 249$ K and were estimated from the critical temperature and pressure given in the reference book.[27] The Lennard-Jones parameters for N_2 as the collision pairs of the xylylperoxy radicals were $\sigma = 3.7$ Å and $\varepsilon = 82$ K, which was taken from ref 28. The Lennard-Jones parameters for collisions between xylylperoxy radicals and N_2 were calculated by the following combination rules,[29]

$$\sigma_{\text{xylylperoxy,N}_2} = 1/2(\sigma_{\text{xylylperoxy}} + \sigma_{\text{N}_2}); \quad \varepsilon_{\text{xylylperoxy,N}_2} = (\varepsilon_{\text{xylylperoxy}} \times \varepsilon_{\text{N}_2})^{1/2}$$

and were used for master equation analysis.

The probability density function for collision energy transfer used was the single exponential-down model:

$$P(E, E') = N(E')^{-1} \times \exp(-(E' - E)/<\Delta E_{\text{down}}>) \qquad \text{for } E < E'$$

where $N(E')$ is a normalization factor, and $<\Delta E_{\text{down}}>$ is the parameter that is equal to an average energy transferred per collision in the single exponential down model. A typical average $<\Delta E_{\text{down}}>$ was set to a standard value 500 cm^{-1} in the present calculations.

3. Results and Discussions

3.1. Isomerization Reactions of the *o*-, *m*-, and *p*-Xylylperoxy Radicals. We have previously reported the theoretical study of the reaction pathways and the kinetics for the benzyl + O_2 reactions.[7] According to our previous work, the benzylperoxy radicals formed by the addition of molecular oxygen isomerize and dissociate into three isomerization channels. In the present calculations, all of these isomerization channels for *o*-, *m*-, and *p*-xylylperoxy radicals were calculated to investigate the relative roles for these isomerization channels. The schematic figures for the isomerization channels of *o*-, *m*-, and *p*-xylylperoxy radicals are shown in Figure 1a, b, and c, respectively. In addition to the isomerization reaction channels (B−D), the dissociation reaction channels (A) forming O atom and the $CH_3C_6H_4CH_2O$ radicals were also calculated for each xylylperoxy isomer, which might play important roles for higher-temperature oxidation of xylyl radicals. For *o*-xylylperoxy radicals, the intramolecular isomerization reaction channels (F), whose transition state was recently calculated by Canneaux et al.,[18] were included in the oxidation reaction scheme (see Figure 1a).

Figures 2 and 3 illustrate the optimized geometries of the transition state structures of *o*-, *m*-, and *p*-xylylperoxy radicals for the isomerization reaction channels (B−D) and of the transition state structure of *o*-xylylperoxy radicals for the isomerization reaction channels (F) at the B3LYP/6-311G(2d,d,p) level of theory, respectively. To compare the optimized transition state structures for the reaction pathways (B−D), we have tabulated the selected bond lengths and angles for these optimized structures. The results were given in Table 1. For comparison, the transition state structures for the isomerization reactions of benzylperoxy radicals calculated by Murakami et al.[7] and Canneaux et al.[8] as well as those for the isomerization reactions for xylylperoxy radicals calculated at the MPW1K method by Canneaux et al.[18] were also tabulated. As shown in Table 1, the bond lengths and angles for the optimized xylylperoxy radicals and those for the transition state structures of **TS1**, **TS2**, and **TS3** had values similar to those for the isomerization reactions of the benzylperoxy radicals, suggesting that methyl substitution for the hydrogen attached to the benzene ring and also the position of the methyl substitution on the benzene ring had little influence on the heats of reaction as well as the barrier heights for these reaction systems.

The bond lengths and angles for the isomerization reactions of *o*-xylylperoxy radicals seemed to have slightly different values, probably due to the repulsions between the neighboring methyl groups, but the differences were found to be very small. Comparing the geometries optimized at the B3LYP/6-311G(2d, d, p) level of theory with those optimized by Canneaux et al.[8,18] using the MPW1K/6-31+G(d, p) level of theory, the structures optimized by the MPW1K method had slightly tight structures. Tokmakov and Lin[30] investigated the capability of various high-level density functional theory and ab initio molecular orbital methods to test the accuracy of the predicted molecular and energetic parameters by calculating the potential energy diagram for the reaction of benzene with OH radicals. They reported that the MPW1K level of theory systematically underestimates bond lengths and overestimates the vibrational frequencies. The same trend of the MPW1K level of theory was also reported in a theoretical study of the thermal decomposition of C_xF_yCO.[31] The present results that the bond lengths predicted by the MPW1K method was smaller than those by the B3LYP method were consistent with their conclusions.

The optimized geometries at the B3LYP/cc-pVDZ level of theory reported by Canneaux et al.[18] were also compared with the present optimized geometries at the B3LYP/6-311G(2d, d, p) level of theory, and it was found that the bond lengths and angles for the geometries optimized at the B3LYP/cc-pVDZ level of theory were almost the same values as those calculated at the B3LYP/6-311G(2d,d,p) level of theory. Thus, it was confirmed that the basis set 6-311G(2d, d,p) was sufficient to obtain the optimized intermediate and transition state structures for the present reaction system. The vibrational frequencies and the rotational constants for these transition state structures were calculated, and it was found from the imaginary vibrational frequencies for these transition states **TS1**, **TS2**, and **TS3** that the tightness of the transition state structures were on the order of **TS1** > **TS2** > **TS3**.

Finally, the relative potential energies for the intermediates and the transition state structures for the reaction pathways (B−D) for *o*-, *m*-, and *p*-xylylperoxy radicals and the reaction pathway (F) for *o*-xylylperoxy radicals were calculated at the higher CBS-QB3 level of theory. Because of the instability for the optimized geometries for the intermediates **4o**, **4m**, and **4p** at the B3LYP level of theory, the total energies for the intermediates **4o**, **4m**, and **4p** were calculated using the CBS-QB3 level of theory with the optimized geometries at the MP2/6-311G(d,p) level of theory, and then the vibrational frequencies as well as the zero-point energies for these intermediates **4o**, **4m**, and **4p** were calculated at the same MP2/6-311G(d,p) level of theory. On the other hand, the transition states for the reaction pathways from **4o** to **7o**, from **4m** to **7m**, and from **4p** to **7p** were not searched because it was expected that the barrier height for this transition state would be low enough to influence on the product branching ratios. The relative potential energies for the intermediate and transition states are given in Table 2. As shown in Table 2, the differences of the relative potential energies for the reaction pathways (A−D) were within 8.5 kJ/mol among *o*-, *m*-, and *p*-xylyl and benzyl radicals, and thus, it was found that the positions of the methyl groups on the aromatic rings (i.e., the differences between the three different isomers of the structures of *o*-, *m*-, and *p*-xylyl radicals) had little influence on the heats of reaction as well as the barrier heights for the xylyl + O_2 reactions. In the case of the *o*-xylylperoxy radical, additional intramolecular isomerization reaction F via the transition state **TS7o** was found to have the lowest activation energy (2.4 kJ/mol), as compared to those for the transition state structures of **TS1**, **TS2**, and **TS3**.

To compare the present results with previous theoretical calculations on the activation barrier heights for the hydrogen transfer reactions of hydrocarbons, we have tabulated the

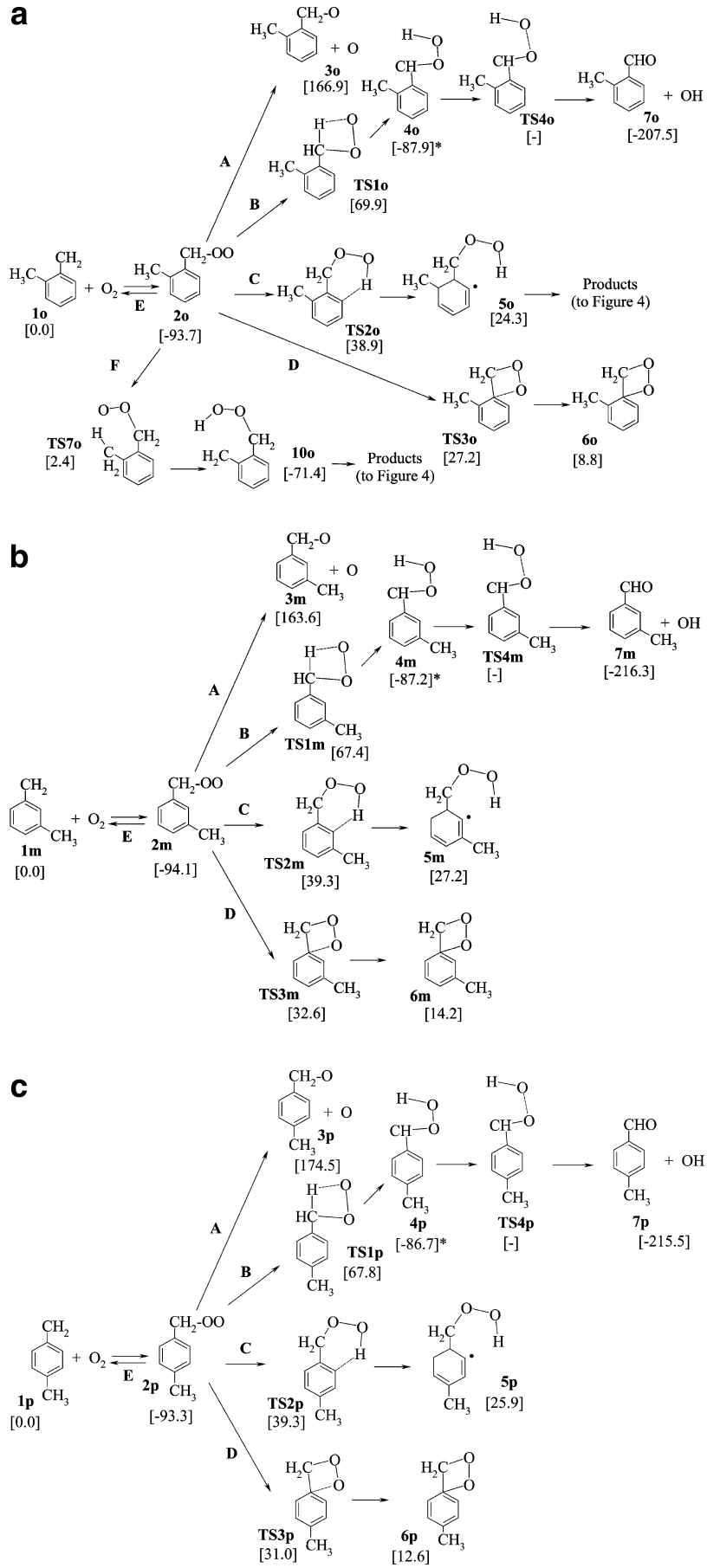

Figure 1. Schematic figures of the possible reaction pathways for the (a) *o*-, (b) *m*-, and (c) *p*-xylyl + O_2 reactions. The number in brackets is the total energies (kJ/mol) relative to the xylyl + O_2 at the CBS-QB3 level of theory. The asterisk indicates that the relative energy was determined by the CBS-QB3 method with the optimized geometries at the MP2/6-311G(d,p) level of theory.

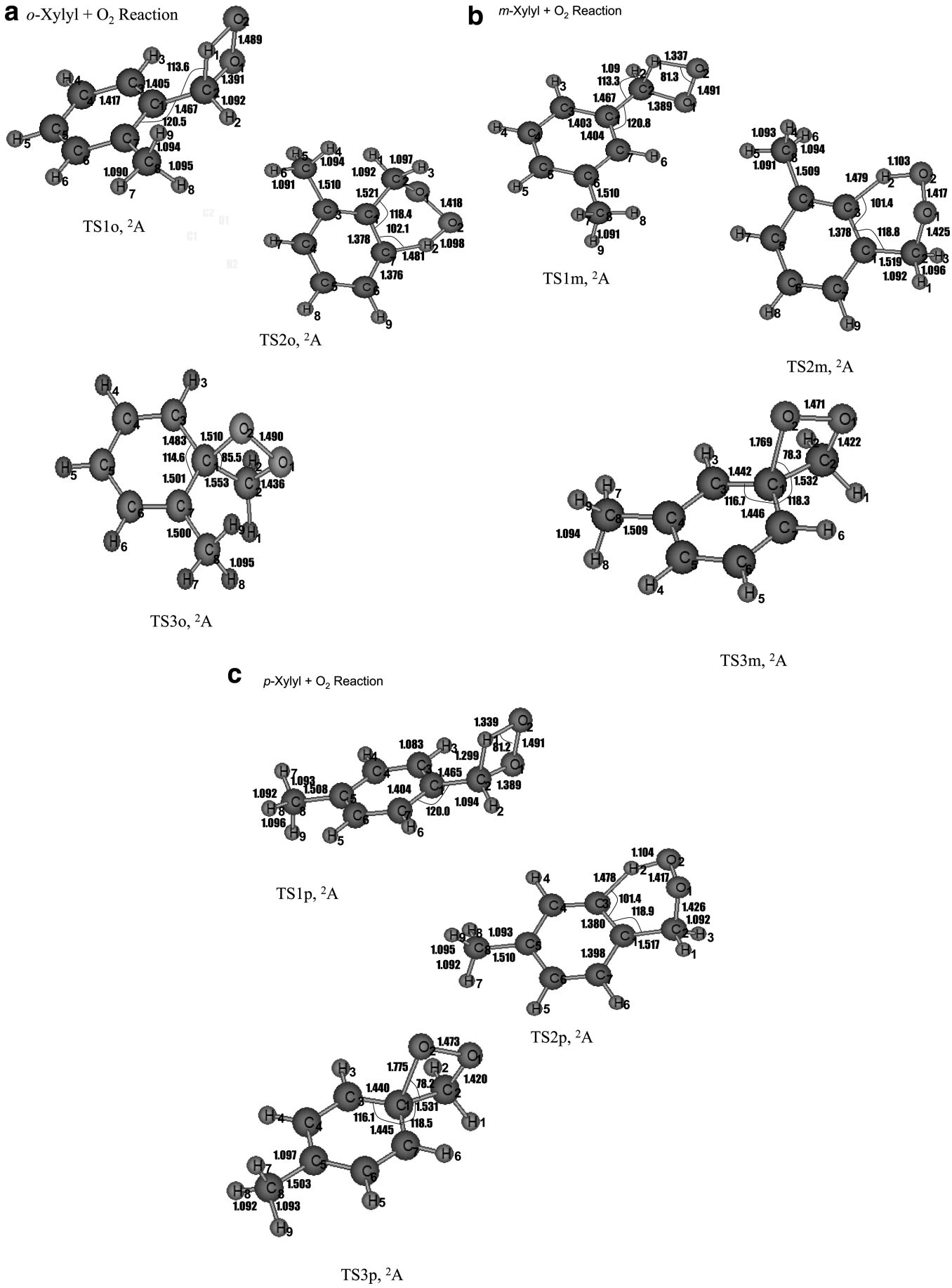

Figure 2. Optimized geometrical parameters of the transition state structure for **TS1**, **TS2**, and **TS3** of the *o*-, *m*-, and *p*-xylyl + O_2 reactions at the B3LYP/6-311G(2d, d, p) level of theory. Bond lengths and angles are in Angstroms and degrees, respectively.

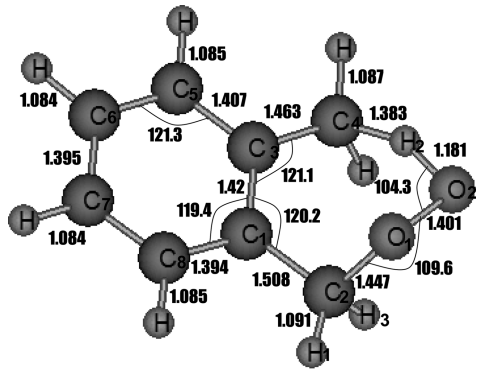

TS7o, ^{2}A

Figure 3. Optimized geometrical parameters of the transition state structure **TS7o** for the intramolecular isomerization between *o*-xylylperoxy radicals and *o*-xylyl hydroperoxy radicals at B3LYP/6-311G(2d, d, p) level of theory. Bond lengths and angles are in Angstroms and degrees, respectively.

TABLE 1: Selected Bond Lengths and Angles of the Transition State Structures at B3LYP/6-311G (2d, d, p) Level of Theory for 2, TS1, TS2, TS3, and TS3 Formed by the Reactions of *o*-, *m*-, and *p*-xylyl + O_2[a,b]

	o-xylyl	*m*-xylyl	*p*-xylyl	benzyl
		2		
R(O1−O2)	1.315 (1.292)	1.315 (1.292)	1.315 (1.292)	1.315 (1.287)
R(C2−O1)	1.478 (1.446)	1.478 (1.446)	1.479 (1.446)	1.478 (1.439)
R(C1−C2)	1.498 (1.492)	1.497 (1.491)	1.496 (1.490)	1.497 (1.491)
R(C2−H1)	1.091 (1.086)	1.091 (1.087)	1.091 (1.087)	1.091 (1.093)
th(O2O1C2)	111.3	111.2	111.2	111.1
th(O1C2C1)	108.7	108.2	108.3	108.2
		TS1		
R(O1−O2)	1.489 (1.444)	1.491 (1.445)	1.491 (1.445)	1.491 (1.445)
R(C2−O1)	1.391 (1.377)	1.389 (1.376)	1.389 (1.370)	1.389 (1.373)
R(C1−C2)	1.467 (1.462)	1.467 (1.462)	1.465 (1.460)	1.467 (1.462)
R(C2−H2)	1.301 (1.295)	1.300 (1.294)	1.299 (1.293)	1.301 (1.299)
th(O2O1C2)	90.3	90.3	90.4	90.3
th(O1C2C1)	117.6	117.8	117.7	117.7
		TS2		
R(O1−O2)	1.418	1.417	1.417	1.417
R(C2−O1)	1.424	1.425	1.426	1.426
R(C1−C2)	1.521	1.519	1.517	1.518
R(C2−H1)	1.092	1.092	1.092	1.092
R(O2−H3)	1.098	1103	1.104	1.101
th(O2O1C2)	107.6	107.3	107.3	107.3
th(O1C2C1)	109.9	109.4	109.2	109.3
		TS3		
R(O1−O2)	1.490	1.471	1.473	1.472
R(C2−O1)	1.436	1.422	1.420	1.421
R(C1−C2)	1.553	1.532	1.531	1.532
R(C2−H1)	1.092	1.094	1.094	1.093
th(O2O1C2)	90.5	92.6	92.7	92.6
th(O1C2C1)	91.3	97.1	97.3	97.1
		TS7		
R(O1−O2)	1.401			
R(C2−O1)	1.447			
R(C1−C2)	1.508			
R(C2−H1)	1.091			
R(O2−H3)	1.093			
th(O2O1C2)	109.6			
th(O1C2C1)	108.3			

[a] The values in parentheses were taken from the previous works (MPW1K/cc-pVDZ in ref 8 and MPW1K/6-31+G(d,p) in ref 18. The bond lengths and angles for the benzyl + O_2 reactions were taken from ref 7. [b] R and th indicates the distance in angstrom and angle in degree.

activation barrier heights of **TS1** and **TS7** from the corresponding xylylperoxy radicals (see Table 3). In all levels of the

TABLE 2: Relative Potential Energies (kJ/mol) for These Transition States Calculated at the Higher Level of CBS-QB3 Theory

reaction	*o*-xylyl	*m*-xylyl	*p*-xylyl	benzyl
1 + O_2	0.0	0.0	0.0	0.0[b]
2	−93.7	−94.1	−93.3	−92.9[b]
3 + O	166.9	163.6	174.5	166.9[b]
TS1	69.9	67.4	67.8	68.6[b]
4 + OH	−87.9[a]	−87.2[a]	−86.7[a]	
7 + OH	−207.5	−216.3	−215.5	−214.6[b]
TS2	38.9	39.3	39.3	42.3[b]
5	24.3	27.2	25.9	28.5[b]
TS3	27.2	32.6	31.0	34.7[b]
6	8.8	14.2	12.6	16.3[b]
TS7	2.4			
10	−71.4			

[a] The total energy for the intermediates **4** was determined by the CBS-QB3//MP2/6-311G(d,p) level of theory. [b] See ref 7.

TABLE 3: Comparison of the Activation Barrier Heights (kJ/mol) of the Transition States Relative to the Corresponding Xylylperoxide Radicals with Various Levels of Calculations

method	**2**	**TS1o**	**TS1m**	**TS1p**	**TS1** (benzyl)	**TS7o**
CBS-QB3	0.0	163.6	161.5	161.1	161.5[a]	96.1
B3LYP/cc-pVDZ	0.0	157.2[b]	154.6[b]	154.4[b]	155.6[c]	90.4[b]
MPW1K/6-31+G(d,p)	0.0	174.7[b]	173.6[b]	173.5[b]	174.7[c]	109.3[b]
CASPT2/ANO-L-VDZP //B3LYP/cc-pVDZ	0.0	146.1[b]	134.4[b]	137.3[b]	137.1[c]	94.6[b]

[a] See ref 7. [b] See ref 18. [c] See ref 8.

calculations, the activation barrier height for **TS7o** is the lowest. The difference in the barrier height between the **TS1o** and **TS7o** was around 65 kJ/mol for the CBS-QB3, B3LYP, and MPW1K methods, but 52 kJ/mol for the CASPT2 method. In addition, the difference in the activation barrier height between **TS1o**, **TS1m** and **TS1p** was below 2 kJ /mol for the CBS-QB3, B3LYP, and MPW1K methods, whereas the difference was as large as 11.7 kJ/mol at the CASPT2 level of theory. Thus, the present CBS-QB3 calculations had the same trend as the previous calculated results of the B3LYP and MPW1K methods by Canneaux et al.,[8,18] but not the CASPT2 method., although CASPT2 can predict the experimentally determined rate constant for reaction pathway B in the benzyl + O_2 reaction system.[10]

Zhu et al.[32] performed the CBS-QB3 calculations of the thermochemical analysis on the intramolecular hydrogen shift reactions of the *n*-butyl and *n*-pentyl hydroperoxy radicals. According to their calculations, the barrier heights of the 4-membered transition states for the isomerization reaction of *n*-butylperoxy and *n*-pentylperoxy radicals were 169.0 and 170.7 kJ/mol, respectively, which are the highest among the other hydrogen shift reactions. Since the barrier heights of the 4-membered transition states for the isomerization reaction of xylylperoxy radicals designated as **TS1** were between 161 and 164 kJ/mol at the same CBS-QB3 level of theory as shown in Table 3, the activation barrier of the 4-membered transition states for the isomerization reaction of xylylperoxy radicals was more than 5 kJ/mol more stable than those for the isomerization reaction of the alkylperoxy radicals (169.0 kJ/mol for *n*-butylperoxy and 170.7 kJ/mol *n*-pentylperoxy radicals). This slight stabilization of the activation barrier may be due to the resonant structure of the aromatic rings attached to the 4-membered transition state structures.

Zhu et al.[32] also reported that the barrier height of the 7-membered transition state (1,6-hydrogen shift reaction) for

the *n*-bytylperoxy and *n*-pentylperoxy radicals was 94.6 and 81.2 kJ/mol at the CBS-QB3 level of theory, respectively. Pfaendtner et al.[33] found that the Evans−Polanyi relationship[34] was shown to capture the activation energy as a function of the heat of reaction for reactions in the 1,5-hydrogen family shift on the basis of the B3LYP/6-311+G(d,p) calculations. The heats of reaction for the 1,6-hydrogen shift of *n*-bytylperoxy and *n*-pentylperoxy radicals reported by Zhu et al.[32] were 72.0 and 57.3 kJ/mol at the CBS-QB3 level, respectively, and therefore, the calculated barrier height of the 7-membered transition state for *n*-bytylperoxy (94.6 kJ/mol) and *n*-pentylperoxy (81.2 kJ/mol) were in accordance with the Evans−Polanyi relationship, although these reactions were not in the family of the 1,5-hydrogen shift, but in the family of the 1,6-hydrogen shift.

In the present calculations, the activation barrier for the reaction of the intramolecular hydrogen shift reaction of *o*-xylylperoxy radicals was determined to be 96.1 kJ/mol at the CBS-QB3 level of theory. Since the calculated heat of reaction for the intramolecular hydrogen shift reaction of *o*-xylylperoxy radicals was 22.3 kJ/mol at the CBS-QB3 level of theory, the activation barrier height for the reaction of the intramolecular hydrogen shift reaction of *o*-xylylperoxy radicals should be much lower than those for the reactions of the 1,6-hydrogen shift of *n*-bytylperoxy and *n*-pentylperoxy radicals, whose heats of reaction were 72.0 and 57.3 kJ/mol at the CBS-QB3 level, respectively, when the Evans−Polanyi relationship held for reactions in the 1,6-hydrogen shift family. However the present results on the calculated activation barrier heights for the reaction of the intramolecular hydrogen shift reaction of *o*-xylylperoxy radicals were 96.0 kJ/mol, which is as high as the barrier heights (94.6 kJ/mol) for the same 7-membered transition state of *n*-butylperoxy radicals.[32] Pfaendtner et al.[33] reported that the Evans−Polanyi relationship differed between the 1,5-hydrogen shift family with and without carbonyl groups, and the existence of the aromatics on the transition state structure might be the reason for such high activation barrier heights as compared with the relatively lower heat of reaction.

3.2. Further Decompositions of the Isomerization Products of o-Xylylperoxy Radicals. Our preliminary objective for the present study was to understand the reasons for the different reactivities among xylene isomers under rapid compression, which was reported by Roubaud et al.[17] Loftus and Satterfield[35] detected phthalan in appreciable quantities during the oxidation of *o*-xylene in air. If the main product of the *o*-xylyl + O_2 reaction was phthalan and OH radicals via **TS7o** and **TS11o**, this would be the reason why *o*-xylene ignited more easily as compared with the other *m*- and *p*-xylenes because OH radicals were known as the chain-propagating carriers and accelerate the ignition delays.[36,37] However, thus far, no detailed experimental and theoretical analysis for the product branching ratios for the reaction of *o*-xylyl + O_2 reaction has not been performed. Thus, we performed detailed quantum chemical calculations on the additional decomposition pathways for the isomerization products of *o*-xylylperoxy radicals.

The schematic figure for these decomposition pathways is illustrated in Figure 4. As shown in Figure 4, OH, HO_2, and CH_2O, which are known as the key species for the chain-propagating or -terminating reactions in low-temperature combustion processes, are produced by these decomposition reactions. Figure 5 illustrates the optimized geometries for these transition states at the B3LYP/6-311G(2d,d,p) level of theory for the *o*-xylyl + O_2 reaction calculated at the CBS-QB3 level of theory.

The reaction pathways forming **8o** and OH radicals via **TS5o** and forming **9o** and CH_2O molecules via **TS6o** have been guessed from the analogous reaction pathways (**TS4** and **TS6** in ref 7), which have already been calculated in the benzyl + O_2 reaction systems.[7] The transition states **TS5o** and **TS6o** are the concerted transition states where bond-dissociation and bond-formation occurs simultaneously. On the other hand, the mechanism for bond-dissociation and bond-formation occurring stepwise was not considered here because these reaction pathways are energetically unfavorable.

The transition structure of **TS5o** forming **8o** and OH molecules from the intermediate **5o** for the reaction of *o*-xylyl + O_2 had the same bond lengths and angles as the corresponding transition state structure for the benzyl + O_2 reaction system.[7] On the other hand, the transition structure of **TS6o** forming **9o** and CH_2O radicals from the intermediate **6o** for the reaction of *o*-xylyl + O_2 gave a slightly different structure as compared with the corresponding transition state structure for the benzyl + O_2 reaction system. For example, the O−O bond length for **TS6o** was 1.724 Å, whereas the O−O bond length for the corresponding transition state for the benzyl + O_2 reaction system was 1.524 Å. The C−O bond lengths of **TS6o** and of the corresponding transition state structure in the benzyl + O_2 reaction system were 1.365 and 1.381 Å, respectively. The difference in the bond lengths and angles between **TS6o** and the corresponding transition state structure for the benzyl + O_2 reaction was probably due to the difference in the heats of reaction for the pathways. That is, the heat of reaction forming **9o** and CH_2O was −283.5 kJ/mol, and therefore, it was more exothermic than the heat of reaction (−273.6 kJ/mol) for the corresponding reaction forming phenoxy radicals and CH_2O molecules in the benzyl + O_2 reaction system. The exothermic nature of the reaction makes the transition state structure productlike, where the O−O bond length became longer and the C−O bond length was near that of the product CH_2O (1.2 Å at the CBS-QB3 level of theory). The heat of reaction forming **8o** and OH radicals was −80.8 kJ/mol, and this value was similar to that in the benzyl + O_2 reaction system (−79.0 kJ/mol), Therefore, the transition structure of **TS5o** forming **8o** and OH radicals from the intermediate **5o** for the reaction of *o*-xylyl + O_2 had the same geometrical parameters as the corresponding transition state structure for the benzyl + O_2 reaction system.

The reaction pathways M−P in Figure 4 played important roles only for the *o*-xylyl + O_2 reactions. **TS8o**, **TS10o**, and **TS11o** are also concerted reactions, and **TS9o** is the simple bond fission reaction simultaneously forming a double C−C bond. According to the CBS-QB3 level of theory, the transition state that has the lowest activation barrier height is **TS11o** (30.5 kJ/mol), and the second lowest is **TS10o** (68.3 kJ/mol). In both reaction pathways O and P, the final product was **14o**, called phthalan, although the reaction pathway (O) has to migrate an oxygen atom to form **14o** from the epoxide structure **13o**. The structure of phthalan **14o** has been experimentally[38] as well as theoretically[39,40] investigated by several researchers. Jeon et al.[39] calculated the conformation properties of phthalan **14o** and concluded that the B3LYP frequency calculations used in the present work were the most accurate theories in predicting the vibrational frequencies and infrared absorption intensities of phthalan **14o**.

The other channels M and N have relatively higher barrier heights (**TS8o**, 180.3 kJ/mol; **TS9o**, 94.2 kJ/mol) as compared with the reaction pathways O and P. The final products for these reaction pathways were benzocyclobutane **11o** and *o*-xylylene

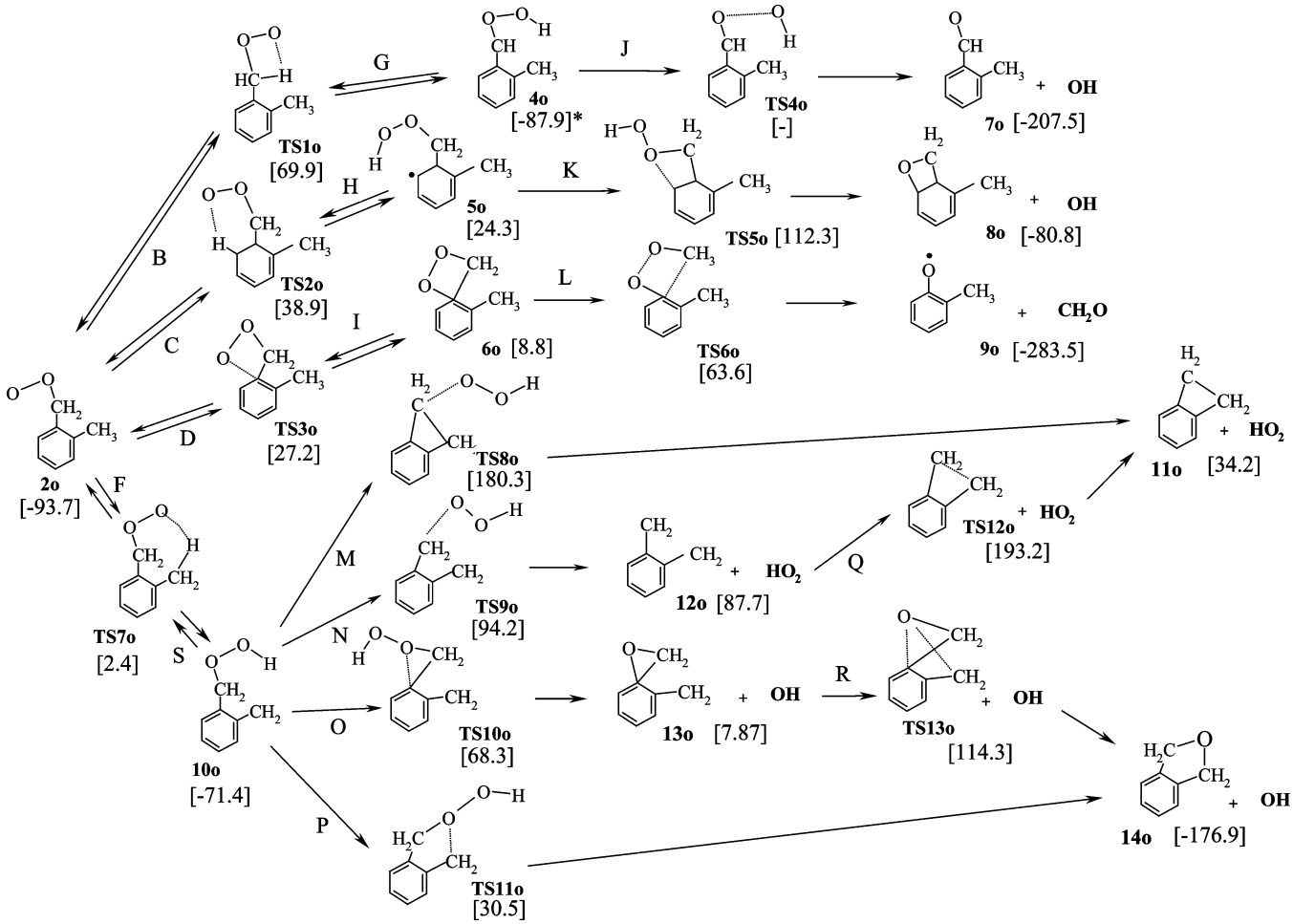

Figure 4. Schematic figures for the possible reaction pathways for the subsequent decomposition reactions of *o*-xylylperoxy radicals. The number in brackets is the total energy (kJ/mol) relative to xylyl + O_2 at the CBS-QB3 level of theory. The asterisk indicates that the relative energy was determined by the CBS-QB3 method with optimized geometries at the MP2/6-311G(d,p) level of theory.

12o, respectively. The transition states for the isomerization reaction between benzocyclobutane **11o** and *o*-xylylene **12o** which serve as the famous examples of the Woodward−Hoffmann rules.[41] Therefore, several researchers have attempted the theoretical calculations for these reactions.[41−43] Guner et al.[42,43] calculated the barrier heights for the isomerization reaction between benzocyclobutane **11o** and *o*-xylylene **12o** and reported that the CBS-QB3 and CASPT2 methods were the most accurate in predicting the activation enthalpies, reaction energies, and transition state structures. According to their calculations, the barrier heights for this reaction at the CBS-QB3 and CASPT2/6-31G(d)//B3LYP/CAS/6-31G(d) levels of theory were 106.3 and 105.5 kJ/mol, respectively. The activation energy for this isomerization reaction was experimentally determined to be 118.8 kJ/mol by Roth et al.[44] The theoretical activation energy was a little bit lower than the experimental value, but relatively good agreement was obtained between experiments and theories. The present results of the activation barrier heights for the isomerization reaction between benzocyclobutane **11o** and *o*-xylylene **12o** using the CBS-QB3 methods was 105.5 kJ/mol, which is in agreement with the previous calculations as well as the experimental results. Finally, we have summarized the potential energy diagram for the *o*-, *m*-, and *p*-xylyl + O_2 reaction in Figure 6a, b, and c, respectively. The present calculations and the comparison with the previous theoretical and experimental values confirm the accuracy of our present calculations on the whole potential energy diagrams for the *o*-, *m*-, and *p*-xylyl + O_2 reaction systems.

3.3. Rate Constants for the Decomposition and Isomerization Reactions of the *o*-Xylylperoxy Radicals. To confirm the important roles of the reaction pathways forming phthalan and OH radicals for the *o*-xylyl radicals with molecular oxygen, the rate constants for all of the multichannel isomerization reactions of *o*-xylylperoxy radicals were calculated using the RRKM theory and the master equation analysis. Since the backward reaction of *o*-xylylperoxy radicals (channel E, Figure 1a)

$$o\text{-}CH_3C_6H_4CH_2OO \rightarrow o\text{-}CH_3C_6H_4CH_2 + O_2$$

also plays a key role in the decomposition reaction of *o*-xylylperoxy radicals, the potential energy profiles for the dissociation reaction pathway E, $o\text{-}CH_3C_6H_4CH_2OO \rightarrow o\text{-}CH_3C_6H_4CH_2 + O_2$, were calculated by fixing the length of the C−O bond from 1.4 to 2.6 Å while all the other geometric parameters were optimized at the B3LYP/6-311G(d,p) level of theory. Calculations of the potential energy profiles for reaction pathway E with different levels of theories were also performed, and it was found that the density functional theory was one of the most accurate and relatively low-cost level of theories that could predict the accurate potential energy profiles for the xylyl + O_2 reaction system. For example, Senosiain et al.[45] and Silva et al.[46] also succeeded in calculating the minimum energy profiles for the OH + acetylene reaction and for the thermal decomposition reaction of the benzyl radical using the B3LYP

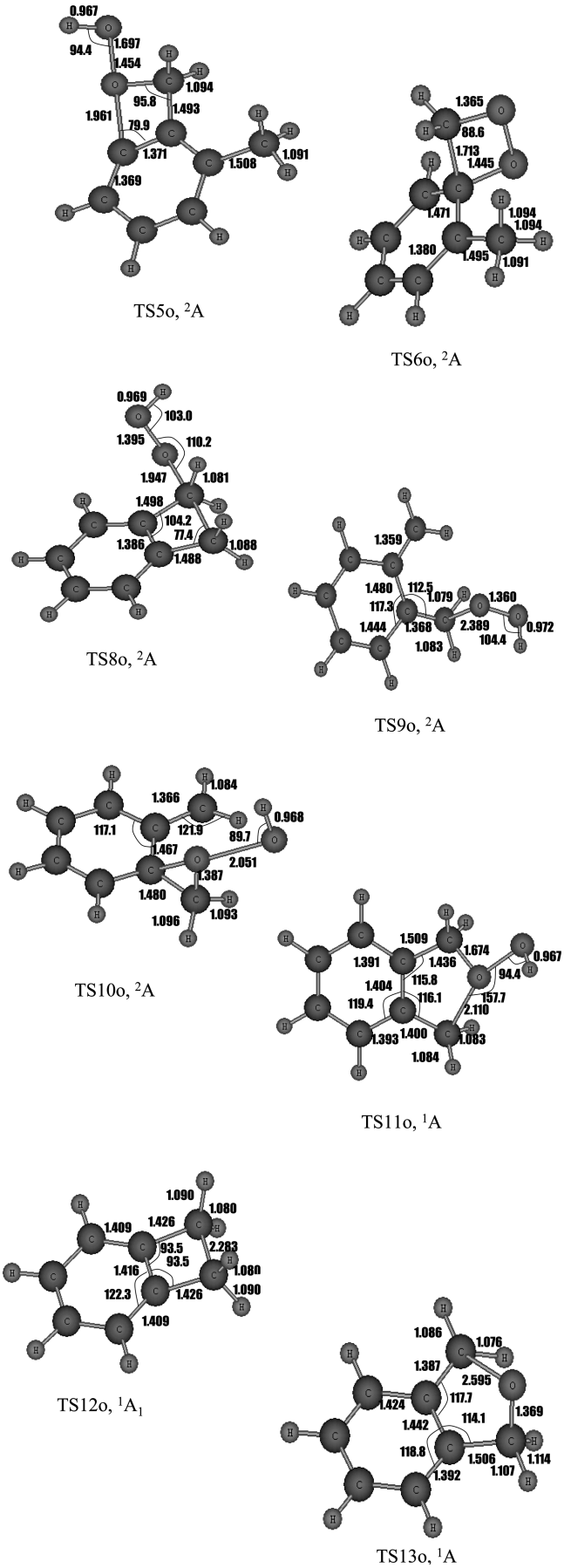

Figure 5. Optimized geometrical parameters of the transition states for the subsequent decomposition reactions of *o*-xylylperoxy radicals at the B3LYP/6-311G(2d, d, p) level of theory. Bond lengths and angles are in Angstroms and degrees, respectively.

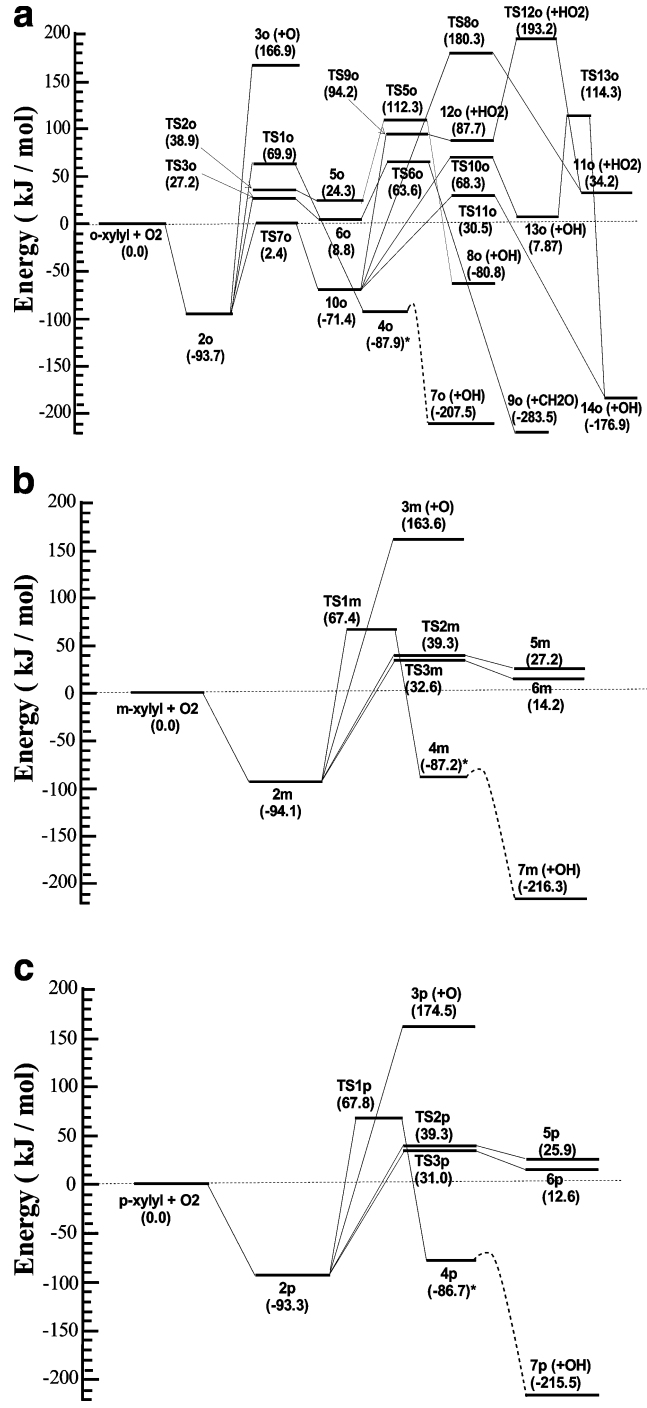

Figure 6. The potential energy surfaces for the reaction of (a) *o*-, (b) *m*-, and (c) *p*-xylyl with molecular oxygen calculated at the CBS-QB3 level of theory (kJ/mol). The numbers in brackets indicate the total energies of the intermediates and the transition states relative to the *o*-, *m*-, and *p*-xylyl + O_2 reaction, respectively.

method, respectively. Therefore, we have adopted the same B3LYP theory to calculate the potential energy profiles for the xylyl + O_2 reaction. The results are shown in Figure 7. A small barrier was found at the C−O bond length 2.37 Å, whose barrier height relative to the reactants *o*-xylyl + O_2 was within 0.4 kJ/mol at the B3LYP/6-311G(d,p) level of theory. The barrier height for the dissociation reaction pathway E, *o*-$CH_3C_6H_4CH_2OO \rightarrow$ *o*-$CH_3C_6H_4CH_2$ + O_2, was so small that the variable transition state must be applied to calculate the rate constant for the backward reactions. The variable transition state was determined by searching the

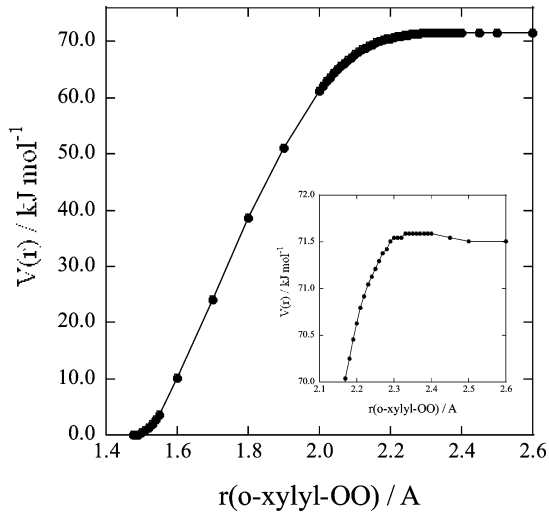

Figure 7. The *o*-xylyl-OO dissociation potential energy profile (kJ mol^{-1}) calculated using the B3LYP density functional with the 6-311G (d,p) basis set. The energy profile was calculated using C_1 symmetry. The insert is the expanded figure of the *o*-xylyl-OO dissociation potential energy profile at the same level of theory.

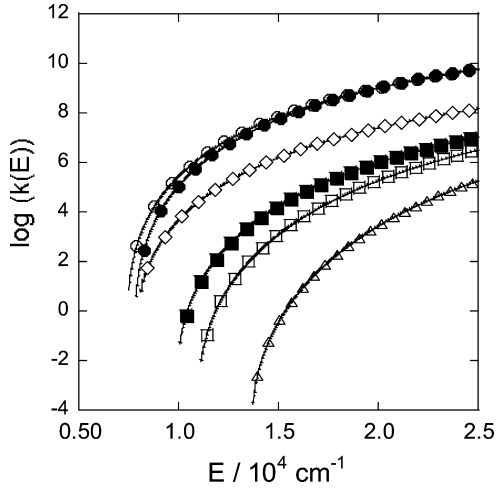

Figure 8. The microcanonical rate constants, $k(E)$, for the backward and isomerization reactions for the o-xylylperoxy radicals as a function of the internal energy above *o*-xylylperoxy radicals. Reaction channel B, Δ; reaction channel C, □; reaction channel D, ■; backward reaction channel E at 300 K, ●; backward reaction channel E at 1500 K, ○; reaction channel F, ◇.

geometries that give the maximum Gibbs free energies at each temperature. The *o*-xylyl-OO distances, relative potential energies for the *o*-xylyl + O_2, rotational constants, and the vibrational frequencies at the variable transition states for each temperature (i.e., 300, 500, 700, 1000, 1200, and 1500 K) used for the RRKM/ME calculations for the backward reaction *o*-$CH_3C_6H_4CH_2OO \rightarrow$ *o*-$CH_3C_6H_4CH_2$ + O_2 are summarized in Table S2 of the Supporting Information.

Figure 8 is the microcanonical rate constants, $k(E)$, for the backward reaction (E) and isomerization reactions B−D and F for the *o*-xylylperoxy radicals as a function of the internal energy above *o*-xylylperoxy radicals. In contrast to the benzylperoxy radicals whose backward reaction was more than 2 orders of magnitude faster than the microcanonical rate constants for the other isomerization reactions, the intramolecular isomerization reaction of *o*-xylylperoxy radicals to form *o*-xylyl hydroperoxy radicals (F) was competitive with the backward dissociation reaction (E). The microcanonical rate constants for isomerization reactions C and D are about 2 orders of magnitude smaller than intramolecuar isomerization reaction F, and that for isomerization reaction B is the smallest.

Using the microcanonical rate constants shown in Figure 8, the master equation analysis was performed at various pressures and temperatures. For the master equation analysis, the single exponential down model was used as the collisional energy transfer between the vibrationally excited xylylperoxy radical and the molecular nitrogen. An average energy transferred per collision $<\Delta E_{down}>$ was set to 500 cm^{-1} in our calculations.[47] The results are summarized in Table 4.

Figure 9 summarized the high-pressure rate constants for these isomerization reactions (B−F) at temperatures between 300 and 1500 K. As shown in Figure 9, backward reaction E is dominant among the five different isomerization reactions of the *o*-xylylperoxy radicals, but intramolecular isomerization pathway F forming the hydroperoxy radicals is also competitive with backward reaction E at all temperature ranges. The rate constant order for these isomerization reactions is as follows: channel E > F > D > C > B, which is the same order as the barrier heights of these isomerization reactions relative to the *o*-xylylperoxy radicals.

Since Canneaux et al.[18] have already reported the high-pressure rate constants for reaction pathways B and F at the CASPT2 level of theory, we have compared them the present calculated rate constants with their values. The results are shown in Figure 10. Although the present calculated high-pressure limit rate constants for reaction channels B and F were in relatively good agreement with the previous CASPT2 calculated rate constants by Canneaux et al.,[18] the high pressure limit rate constants for reaction channel B were a little bit smaller than those by Canneaux et al.,[18] mainly because of the different estimation of the activation barrier heights between the CBS-QB3 method (163.6 kJ/mol) and the CASPT2 method (146.1 kJ/mol). There was only one experimental report on the rate constant for the reaction pathway (B) in benzyl + O_2 reactions, by Ellis et al.[10] No other experimental values of the rate constant for the reaction pathway (B) in the o-xylyl + O_2 reaction have been made available so far. Thus, we have plotted this rate constant for the reaction pathway (B) in benzyl + O_2 reactions by Ellis et al.,[10] as shown in Figure 10. Better agreement with the experimental values obtained by Ellis et al.[10] was found for the rate constant obtained by the CASPT2 method[18] than for the rate constant using the present CBS-QB3 theory, but the disagreements between the predicted rate constants using the CASPT2 theory by Canneaux et al.[18] and the CBS-QB3 theory were within 1 order, and thus, the deviations were relatively small as compared with the previous disagreements between the CBS-QB3 and CASPT2 methods in the case of the benzyl + O_2 reaction.[7,8]

The high-pressure rate constant for reaction pathway F calculated by the present CBS-QB3 method and the previous report by Canneaux et al.[18] are also compared in Figure 10. In this case, the rate constant predicted by the present CBS-QB3 theory was a little bit larger than that by the CASPT2 method, although the predicted activation barrier height by the CBS-QB3 method (96.1 kJ/mol) was larger than the barrier height calculated by the CASPT2 method (94.6 kJ/mol). This might be due to the different estimations of the pre-exponential factors calculated by vibrational frequencies and rotational constants based on the optimized geometries, but again, the differences were so small that we could conclude that the present CBS-QB3 level of theory reproduced the rate constants for the reaction pathways B and F obtained by the CASPT2 method.

TABLE 4: Calculated Rate Constants (s^{-1}) for the Dissociation Reactions of *o*-Xylylperoxy Radicals (channels B−F) and the Bimolecular Rate Constants ($cm^3\ mol^{-1}\ s^{-1}$) for the *o*-Xylyl + O_2 Reaction Forming *o*-Xylylperoxy Radicals

reaction channels	300 K	500 K	700 K	1000 K	1200 K	1500 K
			$P = 0.1$ atm			
2 → **4** (channel B)	0.00×10^{00}	4.06×10^{-06}	1.15×10^{-02}	3.81×10^{-01}	8.61×10^{-01}	1.67×10^{00}
2 → **5** (channel C)	8.17×10^{-12}	9.74×10^{-03}	9.41×10^{00}	1.73×10^{02}	3.33×10^{02}	5.53×10^{02}
2 → **6** (channel D)	1.33×10^{-09}	2.41×10^{-01}	1.45×10^{02}	2.11×10^{03}	3.85×10^{03}	5.90×10^{03}
2 → **1** (channel E)	4.53×10^{-04}	2.58×10^{03}	7.28×10^{05}	7.48×10^{06}	1.35×10^{07}	2.09×10^{07}
2 → **7** (channel F)	7.68×10^{-06}	8.93×10^{01}	2.04×10^{04}	1.94×10^{05}	3.19×10^{05}	4.64×10^{05}
1 + O_2 → **2**	1.80×10^{10}	2.95×10^{10}	1.48×10^{10}	1.58×10^{09}	5.30×10^{08}	1.69×10^{08}
			$P = 1$ atm			
2 → **4** (channel B)	0.00×10^{00}	2.01×10^{-05}	2.82×10^{-01}	2.59×10^{01}	7.53×10^{01}	1.79×10^{02}
2 → **5** (channel C)	8.37×10^{-12}	1.73×10^{-02}	5.91×10^{01}	2.74×10^{03}	6.66×10^{03}	1.34×10^{04}
2 → **6** (channel D)	1.34×10^{-09}	3.41×10^{-01}	5.96×10^{02}	2.05×10^{04}	4.61×10^{04}	8.51×10^{04}
2 → **1** (channel E)	4.53×10^{-04}	2.93×10^{03}	1.73×10^{06}	3.60×10^{07}	7.51×10^{07}	1.30×10^{08}
2 → **7** (channel F)	7.69×10^{-06}	9.98×10^{01}	4.73×10^{04}	9.29×10^{05}	1.83×10^{06}	3.06×10^{06}
1 + O_2 → **2**	1.80×10^{10}	3.35×10^{10}	3.52×10^{10}	7.59×10^{09}	2.95×10^{09}	1.05×10^{09}
			$P = 10$ atm			
2 → **4** (channel B)	0.00×10^{00}	2.92×10^{-05}	1.60×10^{00}	6.59×10^{02}	2.89×10^{03}	9.25×10^{03}
2 → **5** (channel C)	8.38×10^{-12}	1.97×10^{-02}	1.54×10^{02}	2.47×10^{04}	8.51×10^{04}	2.21×10^{05}
2 → **6** (channel D)	1.34×10^{-09}	3.63×10^{-01}	1.20×10^{03}	1.27×10^{05}	3.90×10^{05}	9.06×10^{05}
2 → **1** (channel E)	4.53×10^{-04}	2.98×10^{03}	2.60×10^{06}	1.31×10^{08}	3.45×10^{08}	6.96×10^{08}
2 → **7** (channel F)	7.69×10^{-06}	1.01×10^{02}	7.02×10^{04}	3.37×10^{06}	8.65×10^{06}	1.76×10^{07}
1 + O_2 → **2**	1.80×10^{10}	3.41×10^{10}	5.30×10^{10}	2.76×10^{10}	1.35×10^{10}	5.64×10^{09}
			High-Pressure Limit			
2 → **4** (channel B)	1.07×10^{-16}	3.97×10^{-05}	4.02×10^{00}	2.49×10^{04}	7.65×10^{05}	2.15×10^{07}
2 → **5** (channel C)	1.09×10^{-11}	2.34×10^{-02}	2.55×10^{02}	2.95×10^{05}	4.72×10^{06}	7.68×10^{07}
2 → **6** (channel D)	1.58×10^{-09}	4.26×10^{-01}	1.81×10^{03}	9.86×10^{05}	1.16×10^{07}	1.33×10^{08}
2 → **1** (channel E)	5.28×10^{-04}	3.48×10^{03}	3.44×10^{06}	5.73×10^{08}	4.19×10^{09}	2.80×10^{10}
2 → **7** (channel F)	2.55×10^{-05}	1.18×10^{02}	9.27×10^{04}	1.50×10^{07}	1.13×10^{08}	8.46×10^{08}
1 + O_2 → **2**	2.10×10^{10}	3.98×10^{10}	7.01×10^{10}	1.21×10^{11}	1.65×10^{11}	2.27×10^{11}

Next, the rate constants for the subsequent reactions in Figure 4 were also calculated on the basis of RRKM theory and master equation analysis. The computational results are tabulated in Table 5. Since the shallow well of the intermediate **4o** causes instability of the optimized structures at the B3LYP level of theory, we have considered the rate constant for backward reaction pathway G as negligibly small and that for reaction pathway J was large enough to consider that only the rate constant for the reaction pathway B was the rate-controlling reaction for forming **7o** and OH radicals from intermediates **2o**. As given in Table 5, the subsequent reaction forming the phthalan (**14o**) and OH radicals (**10o** → **14o** + OH, channel P) was one of the major decomposition channels of intermediates **10o** at whole temperature ranges between 300 and 1500 K.

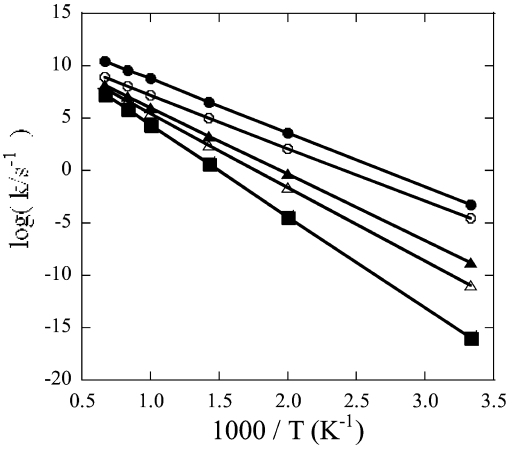

Figure 9. Temperature dependence of the high-pressure limit rate constant for reaction pathways E (●), F (○), D (▲), C (△), and B (■) in the *o*-xylyl + O_2 reaction system.

The rate constants for the other decomposition reactions, such as **5o** → **8o** + OH (channel K) and **6o** → **9o** + CH_2O (channel L), were also comparable to that for reaction pathway **10o** → **14o** + OH (channel P). Therefore, the stationary state approximation was applied to the intermediate species **5o**, **6o**, and **10o** to evaluate the product branching ratios for the *o*-xylyl + O_2 reaction. For simplicity, the subsequent isomerization reactions **12o** → **11o** and **13o** → **14o** were neglected for these stationary state approximations. The results are shown in Figure 11. The calculations were performed at both 0.1 and 10 atm to investigate the effect of the product branching ratios for these reaction channels on the total pressures.

As shown in Figure 11, the phthalan **14o** and OH radicals were the most important dissociation products of the isomerization reactions of *o*-xylylperoxy radicals, which was consistent with previous suggestions by Barnard and Sankey.[15,16] The other dissociation products were more than 2 orders of magnitude smaller than that for **14o** + OH at both 0.1 and 10 atm pressures. The formation of HO_2 by the reaction of **12o** + HO_2 became important at relatively higher temperatures, but still lower than the other dissociation channels forming OH, such as **14o** + OH. The product yields of CH_2O produced by the reaction of **9o** + CH_2O have little temperature dependence and are even lower by more than 1 order of magnitude than the decomposition channel **13o** + OH. Therefore, this decomposition channel from CH_2O, which has an inhibitory effect on the cool flames,[48,49] could be of negligible importance for the low-temperature oxidation of *o*-xylyl + O_2 reactions.

Different reactivities of *o*-xylenes have been suggested at high-temperature flow reactors by Barnard et al.[15,16] Ignition delay measurements of the rapid compression machines have also been suggested by Roubaud et al.[17] On the other hand, no differences in the ignition delay times were observed in a shock

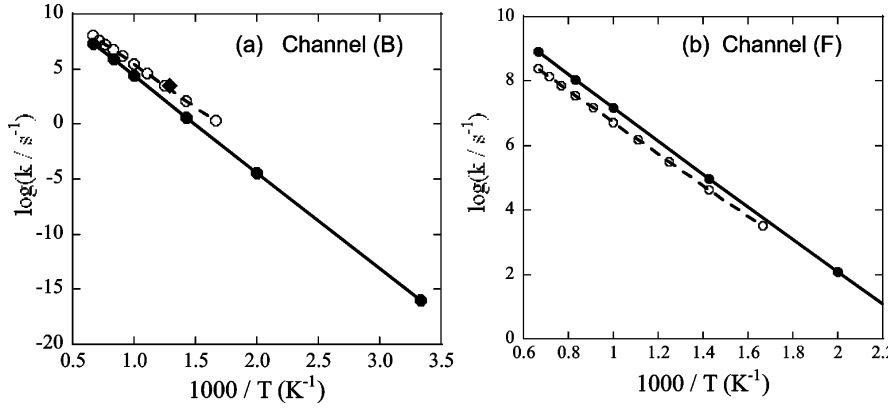

Figure 10. High-pressure limit rate constants for (a) reaction channel B and (b) reaction channel F. Open circles (○) were taken from ref 18. The closed diamond (◆) was taken from ref 10.

TABLE 5: Calculated Rate Constants for the Subsequent Dissociation Reactions of 5o, 6o, 10o and for the Reaction of *o*-Xylyl with O_2 to *o*-Xylyl Peroxide

reaction	300 K	500 K	700 K	1000 K	1200 K	1500 K
5o → **2o** (channel H)	1.90×10^{09}	1.58×10^{10}	4.08×10^{10}	6.56×10^{10}	7.14×10^{10}	7.50×10^{10}
5o → **8o** + OH (channel K)	3.87×10^{-03}	7.66×10^{03}	1.82×10^{06}	1.59×10^{07}	2.34×10^{07}	3.00×10^{07}
6o → **2o** (channel I)	4.24×10^{09}	8.46×10^{10}	3.09×10^{11}	6.91×10^{11}	8.08×10^{11}	8.81×10^{11}
6o → **9o** + CH_2O (channel L)	1.70×10^{03}	1.90×10^{07}	1.08×10^{09}	1.06×10^{10}	1.61×10^{10}	2.04×10^{10}
10o → **2o** (channel S)	3.69×10^{-01}	3.08×10^{04}	9.13×10^{05}	2.80×10^{06}	3.49×10^{06}	4.07×10^{06}
10o → **11o** + HO_2 (channel M)	1.39×10^{-15}	1.08×10^{-03}	1.38×10^{02}	2.49×10^{05}	1.46×10^{06}	3.89×10^{06}
10o → **12o** + HO_2 (channel N)	0.00×10^{00}	0.00×10^{00}	0.00×10^{00}	0.00×10^{00}	0.00×10^{00}	0.00×10^{00}
10o → **13o** + OH (channel O)	5.80×10^{-12}	6.15×10^{-02}	1.28×10^{03}	7.51×10^{05}	3.22×10^{06}	7.14×10^{06}
10o → **14o** + OH (channel P)	1.95×10^{-05}	3.97×10^{02}	5.72×10^{05}	8.46×10^{07}	2.86×10^{08}	5.52×10^{08}
12o → **11o** (channel Q)	1.25×10^{-06}	2.50×10^{01}	3.43×10^{04}	7.61×10^{06}	5.14×10^{07}	2.00×10^{08}
13o → **14o** (channel R)	1.28×10^{-06}	4.06×10^{01}	6.75×10^{04}	1.67×10^{07}	1.06×10^{08}	3.56×10^{08}

tube by Battin-Leclerc et al.[12] The present results that OH radicals and pthalan **14o** were the major decomposition products at whole temperature ranges between 300 and 1500 K seemed to contradict the experimental observations that there were no differences in the ignition delay times among *o*-, *m*-, and *p*-xylenes behind the reflected shockwaves at a temperature range of 1300−1800 K. Hippler et al.[50] reported the thermal decomposition of *p*-xylenes at temperatures of 1200−1600 K behind the reflected shockwaves. Thus, the ignition of the three xylene isomers behind the reflected shockwaves might be initiated by the subsequent oxidation reactions of the thermal decomposition products of xylene isomers, and therefore, this is the reason why little dependence of the ignition delays between xylene isomers was observed as reported by Battin-Leclerc et al.[12] On the other hand, the temperature of the high-temperature flow tube by Barnard et al.[15,16] and the rapid compression machine by Roubaud et al.[17] were very low so that the ring structure of each xylene isomer was present during the oxidation processes, and thus, the different reactivities between the three xylene isomers were observed.

3.4. Rate Constant for the Reaction of *o*-$CH_3C_6H_4CH_2$ + O_2 → *o*-$CH_3C_6H_4CH_3$: Comparison with Experimental Results. In the section 3.2, the potential energy surfaces for the isomerization reactions of *o*-, *m*-, and *p*-xylylperoxy radicals were calculated at the CBS-QB3 level of theory. For modeling xylene combustion, not only the rate constants for the isomerization and the subsequent decomposition reactions of the xylylperoxy radicals, but also those for the primary oxidation step of the xylyl radicals (i.e. xylyl + O_2 reactions) are important. We have already determined the variable transition state for the dissociation reaction pathway E, *o*-$CH_3C_6H_4CH_2OO$ → *o*-$CH_3C_6H_4CH_2$ + O_2 by fixing the length of the C−O bond from 1.4 to 2.6 Å, whereas all the other geometric parameters were optimized at the B3LYP/6-311G(d,p) level of theory. By utilizing these computational results and the equilibrium constant between *o*-$CH_3C_6H_4CH_2OO$ and *o*-$CH_3C_6H_4CH_2$ + O_2 estimated by the geometrical parameters at the B3LYP/6-311G(2d,d,p) level of theory, the rate constants for *o*-xylyl + O_2 at a variety of temperatures and pressures were calculated.

The rate constant for the thermal decomposion of *o*-xylylperoxy radicals **2** to form *o*-xylyl radicals **1** and oxygen molecules is shown in Figure 12. As shown in Figure 12, the rate constants for reaction channel E at pressures of 10−0.1 atm deviated from the high-pressure limit rate constant above 500 K. This is due to the depletion of the collision-induced energized species because of the fast decomposition and slow collision rates at relatively low pressures, which is called the falloff effect in statistical rate theory.[51,52] Comparison of the dissociation rate constant for benzylperoxide to benzyl + O_2 at the high pressure limit is also plotted in Figure 12. As you can see, good agreement of the high-pressure dissociation rate constant between the benzylperoxide and the xylylperoxide was obtained, suggesting that the methyl substitution on the aromatic ring has little influence on the dissociation rate constant.

Finally, the rate constant of the dissociation rate constant for the *o*-xylylperoxide radical was converted to the rate constant of the reaction pathway **1o** + O_2 → **2o** using the equilibrium constant calculated from the optimized geometries and the force constants obtained by the B3LYP method. The results are given in Figure 13. The rate expressions for the reaction **1o** + O_2 → **2o** at high pressure limit were also calculated by the fit to the computational results, and it was determined to be $k = 3.16 \times 10^7\ (T/\mathrm{K})^{1.77} \exp(-126.6\ \mathrm{K}/T)$. The falloff behavior of the rate constant of the reaction pathway **1o** + O_2 → **2o** was also observed above 500 K when the pressures were below 10 atm, but below 500 K, no pressure dependence of the rate constant of the reaction pathway **1o** + O_2 → **2o** was found.

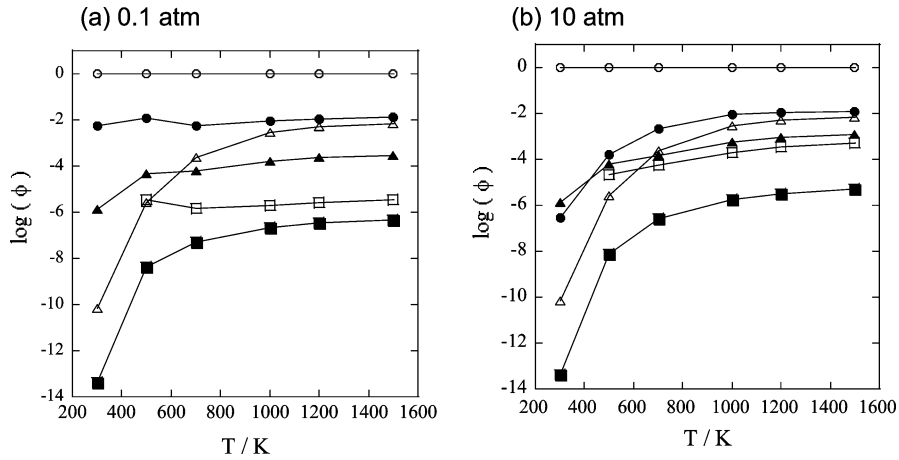

Figure 11. Temperature dependence of the calculated product branching ratios (ϕ) forming phthalan (**14o**) + OH (○), **13o** + OH (●), **12o** + HO_2 (Δ), **9o** + CH_2O (▲), **7o** + OH (□), and **8o** + OH (■) at pressures of (a) 0.1 and (b) 10 atm.

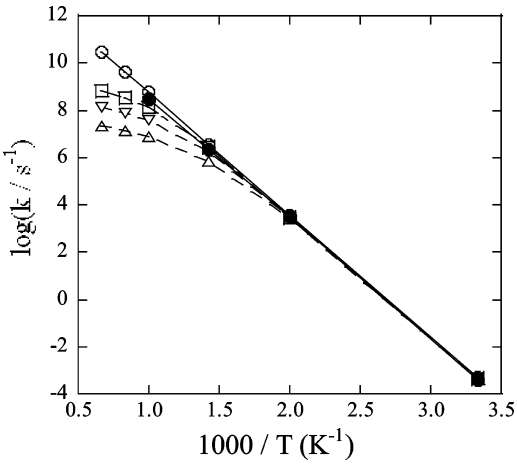

Figure 12. Pressure dependence of the rate constant for the decomposition reaction of *o*-xylylperoxy → *o*-xylyl + O_2 reactions. (a) High pressure limit (○), (b) 10 atm (□), (c) 1 atm (▽), and (d) 0.1 atm (Δ). The closed circles (●) are the rate constants for the decomposition reaction of benzylperoxy → benzyl + O_2 reactions taken from ref 7.

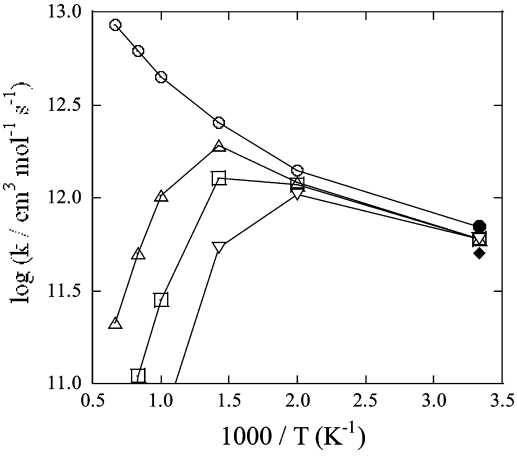

Figure 13. Arrhenius plot of the calculated rate constant for the *o*-xylyl + O_2 reaction: ○, high pressure limit; Δ, $P = 10$ atm; □, $P = 1.0$ atm; ▽, $P = 0.1$ atm; ●, data taken from ref 53; ◆, data taken from ref 54.

There are very few experimental results on the rate constant for the reaction pathway **1o** + O_2 → **2o**. Ebata et al.[53] investigated the rate constant for this reaction by measuring the temporal decay of the absorption for the benzyl- and methyl-substituted benzyl radical after the flash photolysis of the precursors at room temperature. Later, Goumri et al.[54] carried out discharge flow/laser-induced fluorescence experiments and measured the rate constants for the reaction of four benzyl-type radicals with O_2, NO, and NO_2 at room temperature. Both results are also plotted in Figure 13. As shown Figure 13, good agreement between the present theoretical rate constants and the rate constants obtained by experiments was found. However, since there were no rate constants at the higher temperature range, additional fits of our present rate constants to the experiments have not been carried out. Additional experiments are needed to check the accuracy of our theoretical rate predictions.

3.5. Implications for Combustion Chemistry: Low-Temperature-Oxidation of Alkyl Benzenes. According to the previous reports by Roubaud et al.,[17] the autoignition behavior for 11 alkylbenzenes in a rapid compression machine is classified into two classes: The first group was toluene, *m*-xylene, *p*-xylene, and 1,3,5-trimthylbenzene, which ignite only above 900 K and 16 bar. The second group was *o*-xylene, ethylbenzene, 1,2,3-trimethylbenzene, 1,2,4-triethylbenzene, 2-ethyltoluene, etc., which ignite at much lower temperatures and pressures. They did not give any reasons why the ignition behaviors between these alkylbenzenes were classified into two groups.

In the present work, we have proposed that the different ignition behaviors for *o*-, *m*-, and *p*-xylenes were due to the subsequent chain branching reactions of OH radicals formed by the intramolecular isomerization reaction of the *o*-xylylperoxy radicals. Looking at the chemical structures for the alkylbenzenes whose ignition behaviors have been investigated by Roubaud et al.[17] in Figure 14, the alkylbenzenes that have neighboring CH_3 groups belong to group II; on the other hand, those which have the isolated methyl groups belong to group I. It can be expected that the alkylbenzenes, which have neighboring methyl groups, can easily undergo the intramolecular isomerization reaction of the corresponding peroxy radicals with lower activation barriers, and thus, they can produce OH radicals that cause the subsequent chain branching reactions.

On the other hand, the alkylbenzenes that belong to group 1 have only the isolated methyl groups, and therefore, it is difficult for the intramolecular isomerization reaction of the corresponding peroxy radicals to proceed and, thus, also difficult to form OH radicals. That is, the existence and the absence of the intramolecular hydrogen isomerization reactions and the OH-radical formation for the corresponding peroxy radicals determine the reactivities for the alkylbenzenes in a rapid compres-

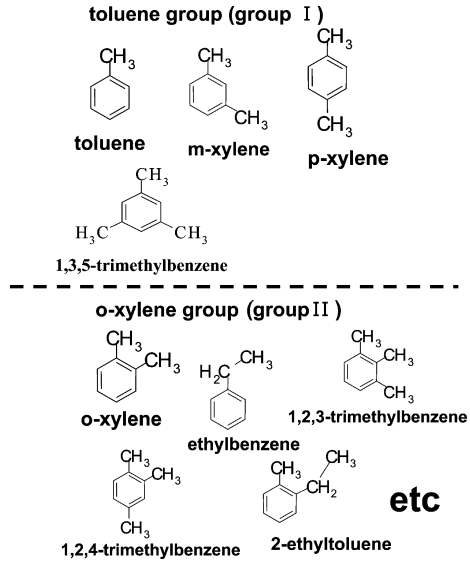

Figure 14. Classification of the alkylbenzenes based on the ignition behaviors under the rapid compression (see ref 17).

sion machine. Once OH radicals are formed after the isomerization reactions of xylylperoxy radicals, the reactive intermediate species such as OH radicals, O atoms, and H atoms will increase exponentially by the chain-branching reactions. Therefore to model the final products in xylene combustion, numerous reactions have to be included in the combustion models, as was pointed out by Silva et al.[55] in the case of toluene combustion. The ignition processes, however, were controlled by relatively fewer numbers of reactions at lower temperatures. It would be easier to predict the phenomena with simpler chemical reaction models.

Rouboud et al.[56] proposed that the addition of molecular oxygen to benzylic-type radicals leads to a double peroxidation and low temperature branching only when the transfer of hydrogen in the isomerization step occurs either from an ortho-alkyl group, or from another carbon atom of the same alkyl chain. They also suggested that the products observed are shown to be consistent with the product mechanism. To confirm their mechanism, quantitative discussions on the final product distributions of the low-temperature oxidation of alkylbenzens using the chemical kinetic models with numerous numbers of chemical reactions will be more important. Additional works on the ignition models for alkylbenzene compounds are underway, and we hope such a quantum chemical approach will give us new insights into such ignition phenomena.

4. Concluding Remarks

The potential energy diagram for *o*-, *m*-, and *p*-xylyl + O_2 reactions was calculated at the CBS-QB3 level of theory, and it was found that the activation barriers and the heats of reaction for these reactions were nearly the same as that for the benzyl + O_2 reaction. The transition states for the intramolecular isomerization and its subsequent reactions were also calculated on the basis of the RRKM and master equation analysis, and it was found that the reaction pathway forming phthalane and OH radicals was the most preferred reaction channel at the whole temperature range of 300−1500 K. The rate constant for the *o*-xylyl + O_2 reaction was calculated by the backward decomposition reaction of *o*-xylylperoxy radicals and the equilibrium constant between *o*-xylyl and *o*-xylylperoxy radicals. It was found that the rate constant for *o*-xylyl + O_2 obtained in the present work could explain the rate constants obtained by the kinetic measurements. Thus, it was suggested that the high reactivity of *o*-xylene compared with toluene and *m*- and *p*-xylenes is due to the high quantum yield of OH radicals in the low-temperature oxidation of *o*-xylyl + O_2 reactions.

Acknowledgment. One of the authors gratefully acknowledges financial support by Sasaki Environmental Technology Foundations. This work was also supported in part by the 21st Century COE Program "Ecological Engineering for Homeostatic Human Activities" at Toyohashi University of Technology from the Ministry of Education, Culture, Sports, Science and Technology. A fruitful discussion with Prof. Mitsuo Koshi, The University of Tokyo, and Prof. William Pitz, Lawrence Livermore National Laboratory, is much appreciated.

Supporting Information Available: The rotational constants and the vibrational frequencies of the transition state structures for the **TS1**, **TS2**, and **TS3** for *o*-, *m*-, and *p*-xylyl + O_2 reactions. The *o*-xylyl-OO distances, relative energies (kJ/mol) to the total energy of *o*-xylylperoxy radicals, the rotational constants, and the vibrational frequencies of the variable transition state of the backward reaction (E) of *o*-$CH_3C_6H_4CH_2OO \rightarrow$ *o*-$CH_3C_6H_4CH_2 + O_2$. Optimized Cartesian coordinate for the transition state structures in Figures 2, 3, and 5 are given. This material is available free of charge via the Internet at http://pubs.acs.org.

References and Notes

(1) Emdee, J. L.; Brezinsky, K.; Glassman, I. *J. Phys. Chem. A* **1992**, *96*, 2151–2161.
(2) Lindstedt, R. P.; Maurice, L. Q. *Combust. Sci. Technol.* **1996**, *120*, 119–167.
(3) Hoyermann, K.; Seeba, J. *Proc. Int. Symp. Combust.* **1994**, *25*, 851–858.
(4) Nelson, H. H.; McDonald, J. R. *J. Phys. Chem.* **1982**, *86*, 1242–1244.
(5) Elmaimouni, L.; Minetti, R.; Sawersyn, J. P.; Devolder, P. *Int. J. Chem. Kinet.* **1993**, *25*, 399–413.
(6) Clothier, P. Q. E.; Shen, D.; Prichard, H. O. *Combust. Flame* **1995**, *101*, 383–386.
(7) Murakami, Y.; Oguchi, T.; Hashimoto, K.; Nosaka, Y. *J. Phys. Chem. A* **2007**, *111*, 13200–13208.
(8) Canneaux, S.; Louis, F.; Ribaucour, M.; Minetti, R.; Bakali, A.; Pauwels, J.-F. *J. Phys. Chem. A* **2008**, *112*, 6045–6052.
(9) Garcia, I.; Uc, V.; Ruiz, M. E.; Smeyers, Y. G.; Bunge, A. V. *J. Mol. Struct. (Theochem)* **1995**, *340*, 149–158.
(10) Ellis, C.; Scott, M. S.; Walker, R. W. *Combust. Flame* **2003**, *132*, 291–304.
(11) Gail, S.; Dagout, P. *Combust. Flame* **2005**, *141*, 281–297.
(12) Battin-Leclerc, F.; Bounaceuer, N.; Glaude, P. A. *Int. J. Chem. Kinet.* **2006**, *38*, 284–302.
(13) Emdee, J. L.; Brezinsky, K.; Glassman, I. *J. Phys. Chem.* **1991**, *95*, 1626–1635.
(14) Wright, F. J. *J. Phys. Chem.* **1960**, *64*, 1944–1950.
(15) Barnard, J. A.; Sankey, B. M. *Combust. Flame* **1968**, *12*, 345–352.
(16) Barnard, J. A.; Sankey, B. M. *Combust. Flame* **1968**, *12*, 353–359.
(17) Roubaud, A.; Minetti, R.; Sochet, L. R. *Combust. Flame* **2000**, *121*, 535–541.
(18) Canneaux, S.; Louis, F.; Ribaucour, M.; Minetti, R.; Bakali, A.; Pauwels, J.-F. *J. Phys. Chem. A* **2009**, *113*, 2995–3003.
(19) Jumgkamp, T. P. W.; Smith, J. N.; Steinfeld, A. *J. Phys. Chem. A* **1997**, *101*, 4392–4401.
(20) Peeters, J.; Nguyen, T. L.; Vereecken, L. *Phys. Chem. Chem. Phys.* **2009**, *11*, 5935–5939.
(21) Kuwata, K. T.; Hasson, A. S.; Dickinson, R. V.; Petersen, E. B.; Valin, L. C. *J. Phys. Chem. A* **2005**, *109*, 2514–2524.
(22) Frisch, M. J. ; Trucks, G. W.; Schlegel, H. B.; Scuseria, G. E.; Robb, M. A.; Cheeseman, J. R.; Montgomery, J. A., Jr.; Vreven, T.; Kudin, K. N.; Burant, J. C.; Millam, J. M.; Iyengar, S. S.; Tomasi, J.; Barone, V.; Mennucci, B.; Cossi, M.; Scalmani, G.; Rega, N.; Petersson, G. A.; Nakatsuji, H.; Hada, M.; Ehara, M.; Toyota, K.; Fukuda, R.; Hasegawa, J.; Ishida, M.; Nakajima, T.; Honda, Y.; Kitao, O.; Nakai, H.; Klene, M.; Li, X.; Knox, J. E.; Hratchian, H. P.; Cross, J. B.; Adamo, C.; Jaramillo, J.;

Gomperts, R.; Stratmann, R. E.; Yazyev, O.; Austin, A. J.; Cammi, R.; Pomelli, C.; Ochterski, J. W.; Ayala, P. Y.; Morokuma, K.; Voth, G. A.; Salvador, P.; Dannenberg, J. J.; Zakrzewski, V. G.; Dapprich, S.; Daniels, A. D.; Strain, M. C.; Farkas, O.; Malick, D. K.; Rabuck, A. D.; Raghavachari, K.; Foresman, J. B.; Ortiz, J. V.; Cui, Q.; Baboul, A. G.; Clifford, S.; Cioslowski, J.; Stefanov, B. B.; Liu, G.; Liashenko, A.; Piskorz, P.; Komaromi, I.; Martin, R. L.; Fox, D. J.; Keith, T.; Al-Laham, M. A.; Peng, C. Y.; Nanayakkara, A.; Challacombe, M.; Gill, P. M. W.; Johnson, B.; Chen, W.; Wong, M. W.; Gonzalez, C.; Pople, J. A. *Gaussian 03*, revision C.02, Gaussian, Inc.: Wallingford CT, 2004.

(23) Montgomery, J. A.; Frisch, M. J.; Ochterski, J. W.; Petersson, G. A. *J. Chem. Phys.* **1999**, *110*, 2822–2827.

(24) Montgomery, J. A.; Frisch, M. J.; Ochterski, J. W.; Petersson, G. A. *J. Chem. Phys.* **2000**, *112*, 6532–6542.

(25) Fenter, F. F.; Noziere, B.; Caralp, F.; Lesclaux, R. *Int. J. Chem. Kinet.* **1994**, *26*, 171–189.

(26) Gilbert, R. G.; Smith, S. C.; Jordan, M. J. T. *UNIMOL Program Suite*, 1993 (calculation of falloff curves for unimolecular and recombination reactions). From the authors at School of Chemistry, Sydney University, NSW 2006, Australia or by e-mail to gilbert@chem.usyd.edu.au.

(27) Poling, B. E.; Prausnitz, J. M.; O'Connell, J. P. *The Properties of Gases and Liquids*; McGraw-Hill: New York, 2000.

(28) Hippler, H.; Troe, J.; Wendelken, H. J. *J. Chem. Phys.* **1983**, *78*, 6709.

(29) Gilbert, R. G.; Smith, S. C. *Theory of Unimolecular and Recombination Reactions*; Blackwell Scientific: Oxford, 1990; p 318.

(30) Tokmakov, I. V.; Lin, M. C. *J. Phys. Chem. A* **2002**, *106*, 11309–11326.

(31) Setoguchi, O.; Kutsuna, S.; Sato, M. *Chem. Phys. Lett.* **2006**, *429*, 360–364.

(32) Zhu, L.; Bozzelli, J. W.; Kardos, L. M. *J. Phys. Chem. A* **2007**, *111*, 6361–6377.

(33) Pfaendtner, J.; Yu, X.; Broadbelt, L. J. *J. Phys. Chem. A* **2006**, *110*, 10863–10871.

(34) Evans, M.; Polany, M. *Trans. Faraday Soc.* **1938**, *34*, 11–29.

(35) Loftus, J.; Satterfield, C. N. J. *J. Phys. Chem.* **1965**, *69*, 909.

(36) Davis, W. M.; Heck, S. M.; Prichard, H. O. *J. Chem. Soc. Faraday. Trans.* **1998**, *94*, 2725–2728.

(37) Prichard, H. O. *Phys. Chem. Chem. Phys.* **2006**, *8*, 4559.

(38) Bondoc, E.; Sakurai, S.; Morris, K.; Chiang, W. Y.; Laane, J. *J. Chem. Phys.* **2000**, *112*, 6700–6706.

(39) Joen, S.; Choo, J.; Kim, S.; Kwon, Y.; Kim, J. Y.; Lee, Y.; Chung, H. *J. Mol. Struct.* **2002**, *609*, 159–167.

(40) Choo, J. *J. Mol. Struct.* **2001**, *597*, 235–240.

(41) Sakai, S. *J. Phys. Chem. A* **2000**, *104*, 11615–11621.

(42) Guner, V.; Khuong, K. S.; Leach, A. G.; Lee, P. S.; Bartberger, M. D.; Houk, K. N. *J. Phys. Chem. A* **2003**, *107*, 11445–11459.

(43) Guner, V.; Khuong, K. S.; Houk, K. N.; Chuma, A.; Pulay, P. *J. Phys. Chem. A* **2004**, *108*, 2959–2965.

(44) Roth, W. R.; Biermann, M.; Dekker, H.; Jochems, R.; Mosselman, C.; Herman, H. *Chem. Ber.* **1978**, *111*, 3892–3903.

(45) Senosiain, J. P.; Klipperstein, S. J.; Miller, J. A. *J. Phys. Chem. A* **2005**, *109*, 6045–6055.

(46) Silva, G.; Cole, J. A.; Bozzelli, J. W. *J. Phys. Chem. A* **2009**, *113*, 6111–6120.

(47) Just, T. H. *Proc. Int. Symp. Combust.* **1994**, *25*, 687–704.

(48) Griffiths, J. F.; Skirrows, G.; Tipper, C. F. H. *Combust. Flame* **1969**, *13*, 195.

(49) Kuwahara, K.; Ando, H.; Fukutani, M.; Ohta, Y. *JSME Int. J. Ser. B* **2005**, *48*, 708.

(50) Hippler, H.; Seisel, S.; Troe, J. *Proc. Int. Symp. Combust.* **1994**, *25*, 875–882.

(51) Troe, J. *J. Chem. Phys.* **1977**, *66*, 4757.

(52) Oref, I.; Tardy, D. C. *Chem. Rev.* **1990**, *90*, 1407–1445.

(53) Ebata, T.; Obi, K.; Tanaka, I. *Chem. Phys. Lett.* **1981**, *77*, 480–483.

(54) Goumri, A.; Elmaimouni, L.; Sawerysyn, J. P.; Devolder, P. *J. Phys. Chem.* **1992**, *96*, 5395–5400.

(55) Silva, G.; Chen, C.; Bozzelli, J. W. *J. Phys. Chem. A* **2007**, *111*, 8663–8676.

(56) Rouboud, A.; Lemaire, O.; Minetti, R.; Sochet, L. R. *Combust. Flame* **2000**, *123*, 561–571.

JP902204A